Fabrication and surface passivation of porous 6H-SiC by atomic layer deposited films

Lu, Weifang; Ou, Yiyu; Petersen, Paul Michael; Ou, Haiyan

Published in:
Optical Materials Express

Link to article, DOI:
10.1364/OME.6.001956

Publication date:
2016

Document Version
Publisher's PDF, also known as Version of record

Fabrication and surface passivation of porous 6H-SiC by atomic layer deposited films

Weifang Lu,* Yiyu Ou, Paul Michael Petersen, and Haiyan Ou

Department of Photonics Engineering, Technical University of Denmark, DK-2800, Lyngby, Denmark
weilu@fotonik.dtu.dk

Abstract: Porous 6H-SiC samples with different thicknesses were fabricated through anodic etching in diluted hydrofluoric acid. Scanning electron microscope images show that the dendritic pore formation in 6H-SiC is anisotropic, which has different lateral and vertical formation rates. Strong photoluminescence was observed and the etching process was optimized in terms of etching time and thickness. Enormous enhancement as well as redshift and broadening of photoluminescence spectra were observed after the passivation by atomic layer deposited Al_2O_3 and TiO_2 films. No obvious luminescence was observed above the 6H-SiC crystal band gap, which suggests that the strong photoluminescence is ascribed to surface state produced during the anodic etching.

OCIS codes: (310.6628) Subwavelength structures, nanostructures; (310.1860) Deposition and fabrication; (310.6870) Thin films, other properties; (250.5230) Photoluminescence.

References and links

1. S. Lau, J. Marshall, and L. Tessler, "Optoelectronic properties of highly conductive microcrystalline SiC produced by laser crystallisation of amorphous SiC," J. Non-Cryst. Solids **198**, 907–910 (1996).
2. K. Wu, Y. Fang, W. Hsieh, J. Ho, W. Lin, and J. Hwang, "High-responsivity porous-SiC thin-film pn junction photodetector," Electron. Lett. **34**(23), 2243–2244 (1998).
3. J. E. Spanier, G. T. Dunne, L. B. Rowland, and I. P. Herman, "Vapor-phase epitaxial growth on porous 6H–SiC analyzed by Raman scattering," Appl. Phys. Lett. **76**(26), 3879–3881 (2000).
4. S. Kim, J. E. Spanier, and I. P. Herman, "Optical transmission, photoluminescence, and Raman scattering of porous SiC prepared from p-type 6H SiC," Jpn. J. Appl. Phys. **39**(1), 5875–5878 (2000).
5. T. Nishimura, K. Miyoshi, F. Teramae, M. Iwaya, S. Kamiyama, H. Amano, and I. Akasaki, "High efficiency violet to blue light emission in porous SiC produced by anodic method," Phys. Status Solidi., C Curr. Top. Solid State Phys. **7**(10), 2459–2462 (2010).
6. H. Ou, Y. Ou, A. Argyraki, S. Schimmel, M. Kaiser, P. Wellmann, M. K. Linnarsson, V. Jokubavicius, J. Sun, R. Liljedahl, and M. Syväjärvi, "Advances in wide bandgap SiC for optoelectronics," Eur. Phys. J. B: Condensed Matter Physics **87**(3), 58 (2014).
7. S. Kamiyama, M. Iwaya, T. Takeuchi, I. Akasaki, M. Syväjärvi, and R. Yakimova, "Fluorescent SiC and its application to white light-emitting diodes," J. Semicond. **32**(1), 013004 (2011).
8. J. S. Shor, I. Grimberg, B. Z. Weiss, and A. D. Kurtz, "Direct observation of porous SiC formed by anodization in HF," Appl. Phys. Lett. **62**(22), 2836–2838 (1993).
9. Y. Shishkin, Y. Ke, R. P. Devaty, and W. J. Choyke, "Fabrication and morphology of porous p-type SiC," J. Appl. Phys. **97**(4), 044908 (2005).
10. T. Matsumoto, J. Takahashi, T. Tamaki, T. Futagi, H. Mimura, and Y. Kanemitsu, "Blue-green luminescence from porous silicon carbide," Appl. Phys. Lett. **64**(2), 226–228 (1994).
11. A. O. Konstantinov, A. Henry, C. I. Harris, and E. Janzén, "Photoluminescence studies of porous silicon carbide," Appl. Phys. Lett. **66**(17), 2250 (1995).
12. Y. Kanemitsu, H. Uto, Y. Masumoto, T. Matsumoto, T. Futagi, and H. Mimura, "Microstructure and optical properties of free-standing porous silicon films: Size dependence of absorption spectra in Si nanometer-sized crystallites," Phys. Rev. B Condens. Matter **48**(4), 2827–2830 (1993).
13. O. Jessensky, F. Müller, and U. Gösele, "Microstructure and photoluminescence of electrochemically etched porous SiC," Thin Solid Films **297**(1-2), 224–228 (1997).
14. D. T. Cao, C. T. Anh, N. T. T. Ha, H. T. Ha, B. Huy, P. T. M. Hoa, P. H. Duong, N. T. T. Ngan, and N. X. Dai, "Effect of electrochemical etching solution composition on properties of porous SiC film," J. Phys. Conf. Ser. **187**, 012023 (2009).
15. A. T. Cao, Q. N. T. Luong, and C. T. Dao, "Influence of the anodic etching current density on the morphology of the porous SiC layer," AIP Adv. **4**(3), 037105 (2014).
16. T. L. Rittenhouse, "Surface-state origin for the blueshifted emission in anodically etched porous silicon carbide," J. Appl. Phys. **95**(2), 490 (2004).

#263004 Received 15 Apr 2016; revised 10 May 2016; accepted 12 May 2016; published 17 May 2016

17. N. I. Berezovska, Y. Y. Bacherikov, R. V. Konakova, O. B. Okhrimenko, O. S. Lytvyn, L. G. Linets, and A. M. Svetlichnyi, "Characterization of porous silicon carbide according to absorption and photoluminescence spectra," Semiconductors **48**(8), 1028–1030 (2014).
18. A. M. Rossi, V. Ballarini, S. Ferrero, and F. Giorgis, "Vibrational and Emission Properties of Porous 6H-SiC," Mater. Sci. Forum **457–460**, 1475–1478 (2004).
19. B. Dou, R. Jia, Y. Sun, H. Li, C. Chen, Z. Jin, and X. Liu, "Surface passivation of nano-textured silicon solar cells by atomic layer deposited Al2O3 films," J. Appl. Phys. **114**(17), 174301 (2013).
20. G. Dingemans and W. M. M. Kessels, "Status and prospects of Al_2O_3-based surface passivation schemes for silicon solar cells," J. Vac. Sci. Technol. A-Vac. Surf. Films **30**(4), 040802 (2012).
21. D. Suh and K. Weber, "Effective silicon surface passivation by atomic layer deposited Al2O3/TiO2stacks," Phys. Status Solidi Rapid Res. Lett. **8**(1), 40–43 (2014).
22. I.-S. Yu, Y.-W. Wang, H.-E. Cheng, Z.-P. Yang, and C.-T. Lin, "Surface Passivation and Antireflection Behavior of ALD on n-Type Silicon for Solar Cells," Int. J. Photoenergy **2013**, 1–7 (2013).
23. H. Kang, C.-S. Lee, D.-Y. Kim, J. Kim, W. Choi, and H. Kim, "Photocatalytic effect of thermal atomic layer deposition of TiO2 on stainless steel," Appl. Catal. B **104**(1-2), 6–11 (2011).
24. A. Richter, J. Benick, M. Hermle, and S. W. Glunz, "Reaction kinetics during the thermal activation of the silicon surface passivation with atomic layer deposited Al_2O_3," Appl. Phys. Lett. **104**(6), 061606 (2014).
25. M. Otto, M. Kroll, T. Käsebier, R. Salzer, A. Tünnermann, and R. B. Wehrspohn, "Extremely low surface recombination velocities in black silicon passivated by atomic layer deposition," Appl. Phys. Lett. **100**(19), 191603 (2012).
26. A. Dillon, A. Ott, J. Way, and S. George, "Surface chemistry of Al_2O_3 deposition using Al $(CH_3)_3$ and H_2O in a binary reaction sequence," Surf. Sci. **322**(1-3), 230–242 (1995).
27. P. Newby, J.-M. Bluet, V. Aimez, L. G. Fréchette, and V. Lysenko, "Structural properties of porous 6H silicon carbide," Phys. Status Solidi., C Curr. Top. Solid State Phys. **8**(6), 1950–1953 (2011).
28. N. Batra, J. Gope, J. Vandana, J. Panigrahi, R. Singh, and P. K. Singh, "Influence of deposition temperature of thermal ALD deposited Al_2O_3 films on silicon surface passivation," AIP Adv. **5**(6), 067113 (2015).
29. M. Cameron, I. Gartland, J. Smith, S. Diaz, and S. George, "Atomic layer deposition of SiO_2 and TiO_2 in alumina tubular membranes: pore reduction and effect of surface species on gas transport," Langmuir **16**(19), 7435–7444 (2000).
30. I. Iatsunskyi, M. Kempiński, M. Jancelewicz, K. Załęski, S. Jurga, and V. Smyntyna, "Structural and XPS characterization of ALD Al_2O_3 coated porous silicon," Vacuum **113**, 52–58 (2015).
31. W.-J. Lee and M.-H. Hon, "Space-Limited Crystal Growth Mechanism of TiO_2 Films by Atomic Layer Deposition," J. Phys. Chem. C **114**(15), 6917–6921 (2010).
32. C. Jin, B. Liu, Z. Lei, and J. Sun, "Structure and photoluminescence of the TiO_2 films grown by atomic layer deposition using tetrakis-dimethylamino titanium and ozone," Nanoscale Res. Lett. **10**(1), 95 (2015).
33. J. Fan, H. Li, J. Wang, and M. Xiao, "Fabrication and photoluminescence of SiC quantum dots stemming from 3C, 6H, and 4H polytypes of bulk SiC," Appl. Phys. Lett. **101**(13), 131906 (2012).
34. X. Zhang, T. Lin, P. Zhang, J. Xu, S. Lin, L. Xu, and K. Chen, "Highly efficient near-infrared emission in Er^{3+} doped silica films containing size-tunable SnO_2 nanocrystals," Opt. Express **22**(1), 369–376 (2014).
35. D. N. Goldstein, J. A. McCormick, and S. M. George, "Al_2O_3Atomic Layer Deposition with Trimethylaluminum and Ozone Studied by in Situ Transmission FTIR Spectroscopy and Quadrupole Mass Spectrometry," J. Phys. Chem. C **112**(49), 19530–19539 (2008).
36. W. D. de Boer, D. Timmerman, K. Dohnalová, I. N. Yassievich, H. Zhang, W. J. Buma, and T. Gregorkiewicz, "Red spectral shift and enhanced quantum efficiency in phonon-free photoluminescence from silicon nanocrystals," Nat. Nanotechnol. **5**(12), 878–884 (2010).

1. Introduction

Silicon carbide (SiC) is a highly chemical resistant semicondutor material at room temperature. Porous SiC is a potentially attractive material for light emitting diodes (LEDs), photodetectors, sensors and substrate for monocrystalline SiC epitaxy [1–4]. Among these applications, porous SiC has potential to realize fluorescent SiC based white LEDs [5–7]. Porous SiC was first fabricated by Shor et al. [8] by using anodic etching method, which anodizing single crystal n-type 6H-SiC in hydrofluoric acid and under UV illumination. Since then, a lot of studies of porous SiC have been reported with specific changes in morphology, optical transmittance and photoluminescence (PL) properties after the formation of porous structures in both 6H and 4H n-type or p-type SiC wafers [4, 5, 9–15].

The wide difference of porous morphology often exists and agreement on the explanation of the PL spectra in porous SiC has not been reached yet. To date, there are mainly two different interpretations: a) quantum confinement effect [5]; b) surface-state upon anodic etching [4, 12, 16–18]. However, the large surface area also leads to an enhanced non-radiative recombination rate due to the surface damage caused by etching process [19]. It is known that the Al_2O_3 and TiO_2 films are widely used as passivation materials with high melting point, excellent mechanical property and chemical stability [20–26]. Furthermore,

#263004 Received 15 Apr 2016; revised 10 May 2016; accepted 12 May 2016; published 17 May 2016

atomic layer deposition (ALD) is a modernized deposition method for surface passivation, which allows homogeneity to be achieved on complex structures [7]. Thus, coating porous SiC by ALD Al_2O_3 or TiO_2 could be an ideal way to realize surface passivation and increase the PL intensity. To our knowledge, a study of the passivation effect on different thickness of porous 6H-SiC by using atomic layer deposited Al_2O_3 and TiO_2 films has not been reported yet, and the luminescence mechanism is still quite blurring.

In this work, we investigated the passivation effect of ALD Al_2O_3 and TiO_2 on porous 6H-SiC. For comparison, we also present the preliminary result of the effect of anodic etching time on porous 6H-SiC structures. The morphology, reflectance, transmittance and PL properties were investigated first. Then, the porous samples passivated by Al_2O_3 and TiO_2 films, respectively, were fabricated and the passivation effects on different thickness of porous layer were analyzed.

2. Experiments and results

The single-crystal 6H-SiC (n-type) samples used in this study were Si-face polished substrate with a thickness of 250 μm supplied by SiCrystal AG (Germany). The substrate was doped with nitrogen and had a resistivity of around 0.1 Ω cm. Ohmic contacts on the back side of SiC substrate were formed by evaporation of 200 nm thick aluminum (Alcatel SCM 600 E-beam and sputtering deposition system). To obtain pores in 6H-SiC, samples were mounted in a Teflon etch-cell with a platinum (Pt) counter electrode. The etching solution is hydrofluoric acid (HF) diluted solution with a concentration of 5 wt. %.

The anodic etching was done under yellow light environment and all the samples were etched at constant current density of 2 mA/cm^2. During the electroetching process, the hydroxide ions arrived at the surface of 6H-SiC and partially oxidized 6H-SiC to form SiO_2 and CO_2. Simultaneously, SiO_2 reacted with HF and formed soluble H_2SiF_6. The electrochemical etching processes were proposed as follows [5]:

$$SiC + 6OH^- \rightarrow SiO_2 + CO_2 + 2H_2O + 2H^+ + 8e \quad (1)$$

$$SiO_2 + 6F^- + 2H^+ \rightarrow H_2SiF_6 + 2H_2O + 4e^- \quad (2)$$

6H-SiC samples a, b, c and d were prepared with a etching time of 60, 150, 260, and 360 minutes, respectively.

2.1 Morphology of porous 6H-SiC

The morphology of porous 6H-SiC was investigated by scanning electron microscopy (SEM). Cross-sectional SEM images taken at different depths of sample d are shown in Fig. 1. The total etching time for this sample is 360 min. It can be obviously seen that there are holes around 63nm on the surface, as shown in Fig. 1(a). The formed thickness of porous layer is 38.88 μm, which consists of a layer of ultra-small triangular pores (top layer), a layer of sparse dendritic pores (middle layer) and a thick layer of dense dendritic pores (bottom layer). As one can see that, not only the porosity changes but also there are obvious boundaries between two different porous layers, as shown in Fig. 1(c) and 1(d). The porosity of the electrochemically etch 6H-SiC crystal is quite non-uniform throughout the porous layer. The pore in the top layer is quite small and the size gradually increases towards the bottom layer. However, the formed channels branch horizontally and also tend to propagate perpendicularly to the basal plane. Finally, the channels are occasionally intersected with each other.

#263004 Received 15 Apr 2016; revised 10 May 2016; accepted 12 May 2016; published 17 May 2016

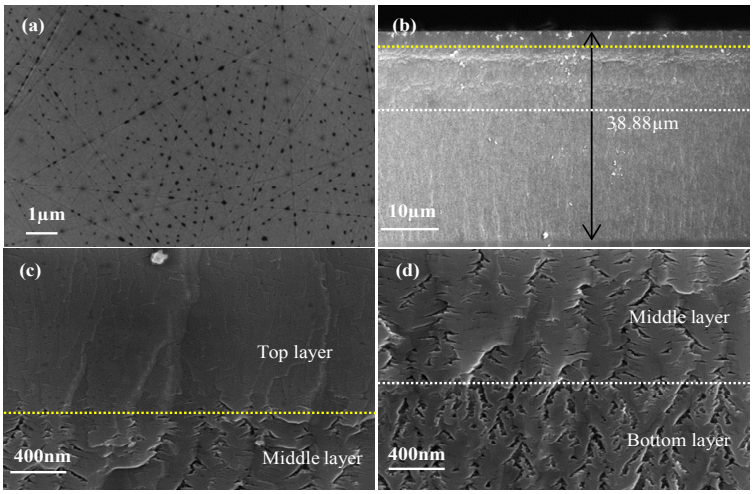

Fig. 1. Planar and cross-sectional view of SEM images of sample d: (a) the hole on the surface is around 63nm and (b) the overview of the porous layer consisting of three layers with a total thickness of 38.88 μm, (c) the boundary between top layer and middle layer, and (d) the boundary between the middle and bottom layer.

Samples a, b and c produced under the same conditions etched for 60, 150 and 260 min respectively also have three different layers with the same structure profiles and pore size as sample d. The thicknesses of the porous layer for sample a, b, c, and d were 2.65 μm, 22.14 μm, 24.74 μm and 38.88 μm, respectively. The photographs and corresponding SEM images of the bottom layer area are shown in Fig. 2. The dark circles in the photographs are the porous area, which becomes uneven with etching time increased.

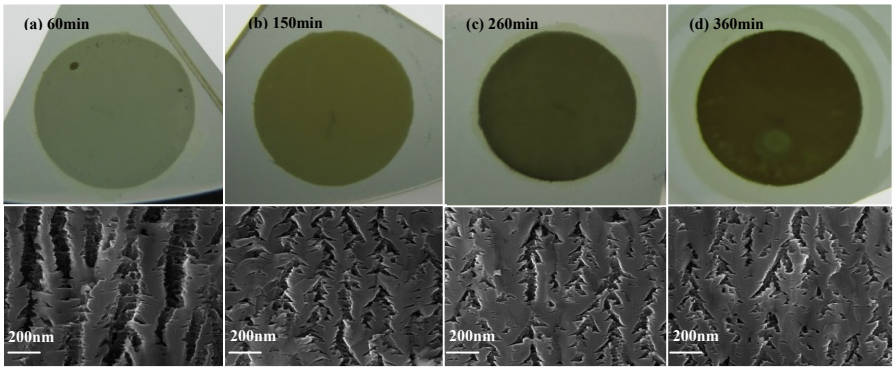

Fig. 2. Photographs of porous SiC with different etching time (a) 60 min, (b) 150 min, (c) 260 min and (d) 360 min. The corresponding cross-sectional SEM images are also shown underneath, taken near the interface between the porous layer and the substrate.

The relationship between the porous thickness and etching time is shown in Fig. 3. Assuming, the anodic etching process is anisotropic, i.e., there are vertical and lateral etching, which competed with each other. As the anodic etching time increases, the relative thickness of the dendritic layer (compared with the top layer) also increases, as shown in Fig. 3. This indicates that the small triangular pores in the top layer is the initial stage of the dendritic pore structures [27]. As the porous layer became thicker, the formed SiO_2 in deep layer could not be dissolved efficiently, which could block the vertical etching.

#263004 Received 15 Apr 2016; revised 10 May 2016; accepted 12 May 2016; published 17 May 2016

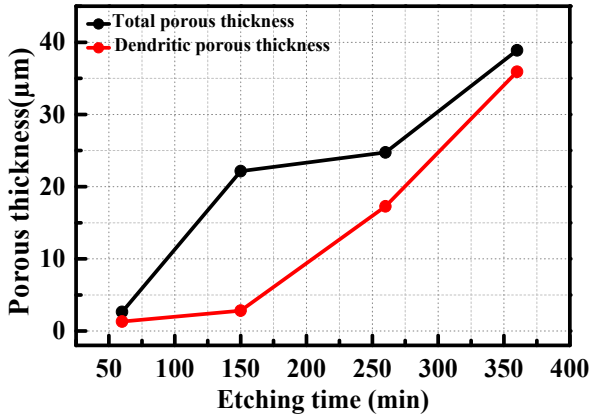

Fig. 3. Relationship of porous thickness and dendritic thickness with etching time for 6H-SiC: the trend for total porous layer and dendritic layer (middle + bottom layer) was plotted for analyzation.

2.2 Reflectance and transmittance in porous 6H-SiC

In order to investigate the optical properties of the porous 6H-SiC samples, reflectance and transmittance spectra have been measured by using a calibrated integrating sphere system (Gooch & Housego OL 700-71). The results are shown in Fig. 4. Figure 4(a) shows that the reflectance of porous samples has been increased over the wavelength range from 380 to 780 nm, compared with the flat reference sample. The reflectance also increased with the increasing of anodic etching time due to the reflection on sidewall of pores. It can be noticed that the reflectance of sample a is higher than that of sample b, which may be related to the larger dendritic structures, as shown in Fig. 2. The maximum value of reflectance red shifts from 475 to 550 nm as the anodic etching time increased. This phenomenon is in accordance with the photographs in Fig. 2, that is, the longer wavelength could be reflected with the porous thickness increasing.

As shown in Fig. 4(b), the transmittance of porous samples has been significantly decreased compared to the flat sample, especially for samples c and d. After anodic etching, the porous 6H-SiC layers are still crystalline and they should be transparent for the wavelength above bandgap. However, the observed low transmittance performance of porous 6H-SiC sample is attributable to the enormous surface states [4].

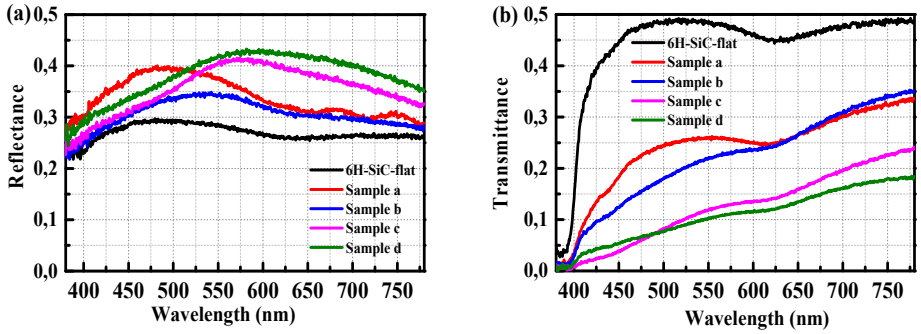

Fig. 4. Comparison of the measured (a) reflectance and (b) transmittance spectra for the flat 6H-SiC sample and the porous samples a, b, c and d.

#263004 Received 15 Apr 2016; revised 10 May 2016; accepted 12 May 2016; published 17 May 2016

2.3 Atomic layer deposited Al_2O_3 and TiO_2 films

The surface state may also contain non-radiative recombination component, thus surface passivation should be introduced to improve the light emitting properties. In order to passivate the enormous surface of the porous samples, ALD (Model R200, Picosun, Finland) Al_2O_3 and TiO_2 films were used to cover the pore surface. The Al_2O_3 thin films were deposited on porous samples using H_2O and trimethylaluminium (TMA: $Al(CH_3)_3$) gases as precursor materials for the oxygen and aluminum, respectively. The reaction took place in cycles. In this work, one deposition cycle included 0.1 s pulse of TMA, 3 s N_2 purge, 0.1 s H_2O exposure and followed by 3 s N_2 purge. The surface chemical reaction of Al_2O_3 deposition consists of two half reactions [26, 28]:

$$1^{st}\,\text{half}-\text{reaction}: \quad \text{Al}-\text{OH}+\text{Al}\left(\text{CH}_3\right)_3 \rightarrow \text{Al}-\text{O}-\text{Al}\left(\text{CH}_3\right)_2+\text{CH}_4 \qquad (3)$$

$$2^{nd}\,\text{half}-\text{reaction}: \ \text{Al}-\text{O}-\text{Al}\left(\text{CH}_3\right)_2+2\text{H}_2\text{O} \rightarrow \text{Al}-\text{O}-\text{Al}\left(\text{OH}\right)_2+2\text{CH}_4 \qquad (4)$$

As the similar deposition process for TiO_2 thin films, the reaction is also divided into the following two half-reactions [29]:

$$1^{st}\,\text{half}-\text{reaction}: \text{Ti}-\text{OH}+\text{TiCl}_4 \rightarrow \text{Ti}-\text{O}-\text{TiCl}_3+\text{HCl} \qquad (5)$$

$$2^{nd}\,\text{half}-\text{reaction}: \text{Ti}-\text{Cl}+\text{H}_2\text{O} \rightarrow \text{Ti}-\text{OH}+\text{HCl} \qquad (6)$$

The desired Al_2O_3 or TiO_2 thickness can be obtained by controlling the number of ALD deposition cycles. In this paper, a 20 nm (200 cycles) thick Al_2O_3 layer was deposited on porous samples at 160 °C with a growth rate of 1 Å/cycle. For comparison, a same thickness of TiO_2 (410 cycles) was deposited on another batch of samples at 150 °C with a deposition rate of 0.49 Å/cycle. It is well known, at the deposition temperature around 150°C, Al_2O_3 and TiO_2 are definitely in amorphous phase [30–32]. It should be mentioned that the ALD deposited Al_2O_3 and TiO_2 films contain O-H bond, which has been confirmed in [19, 24–26, 29]. A post-deposition annealing was performed at 350 °C for 5 min in N_2 (10 sccm) environment by rapid thermal annealing (RTA, Jipelec) for all the samples in order to activate the passivation layer.

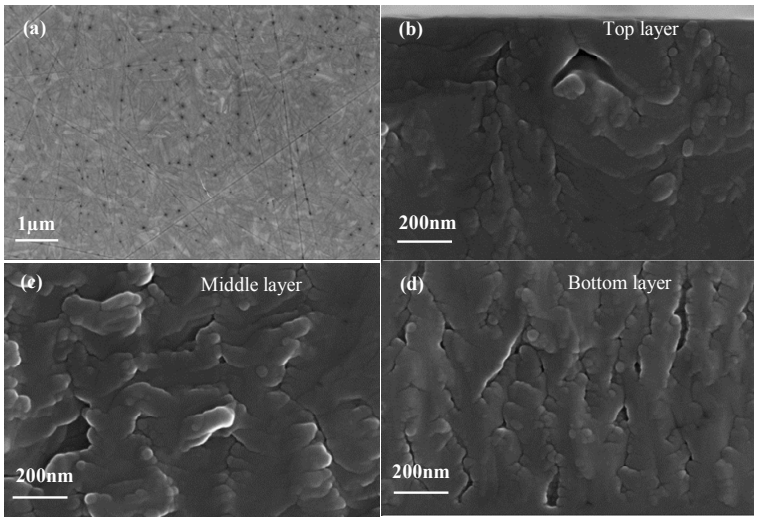

Fig. 5. Planar and cross-sectional SEM images of sample d (360 min): (a) the surface holes, (b) top layer, (c) middle layer and (d) bottom layer covered with 20 nm thick TiO_2.

The plan and cross-sectional SEM images of sample d with 20 nm thick TiO_2 are shown in Fig. 5. The holes on the surface are still clealy visible, which haven't been blocked by 20nm films. However, the TiO_2 films could conformally coat and almost fulfill the pores in

#263004 Received 15 Apr 2016; revised 10 May 2016; accepted 12 May 2016; published 17 May 2016

deep layers. If the surface porous layer are completely filled by Al_2O_3 or TiO_2, the penetration of precursor molecules inside the pores should decrease, i.e. the pores closed. The morphology of porous sample covered with 20 nm thick Al_2O_3 is similar to that of TiO_2.

2.4 Photoluminescence and passivation effect of ALD Al_2O_3 and TiO_2 films

PL measurements were carried by using a 375 nm laser as excitation source coupled into a microscope. In the present experiments, the excitation light was focused on the sample surface through the microscope with a dichroic mirror and a long working distance 20x objective lens. The luminescence signal was filtered by a long-pass filter with cutoff wavelength at 420nm and collected by an optical spectrometer (CAS 140 B, Compact Array Spectrometer, Instrument System). Figure 6(a) shows the PL spectra for the flat and porous 6H-SiC samples a-d. It is apparent that the original flat sample has very weak light emitting, but all the porous samples have a strong luminescence peak around 535 nm with a full width at half maximum (FWHM) of 160 nm. For 6H-SiC, the exciton Bohr radius is 0.7 nm [33]. The diameter size of the current porous samples are above 6 nm, which is much greater than the exciton Bohr diameter of 6H-SiC, so the PL in porous samples should not be dominated by quantum size effects. And it could be attributed to surface states on the large internal surface of porous structures, such as oxygen vacancies and dangling bonds [13, 16, 34]. Surface states generally formed on the porous samples were associated with the chemical reaction during anodic etching process [16–18]. Surface states also contained non-radiative recombination component which need to be passivated to increase the radiative recombination component. The PL performance of porous samples a, b, c and d passivated by Al_2O_3 or TiO_2 is investigated, and their PL spectra plotted in the visible light spectral range are illustrated in Fig. 6(b) and 6(c), respectively. PL spectra of porous samples show a broadening and red shift with respect to the spectra of porous 6H-SiC samples without surface passivation.

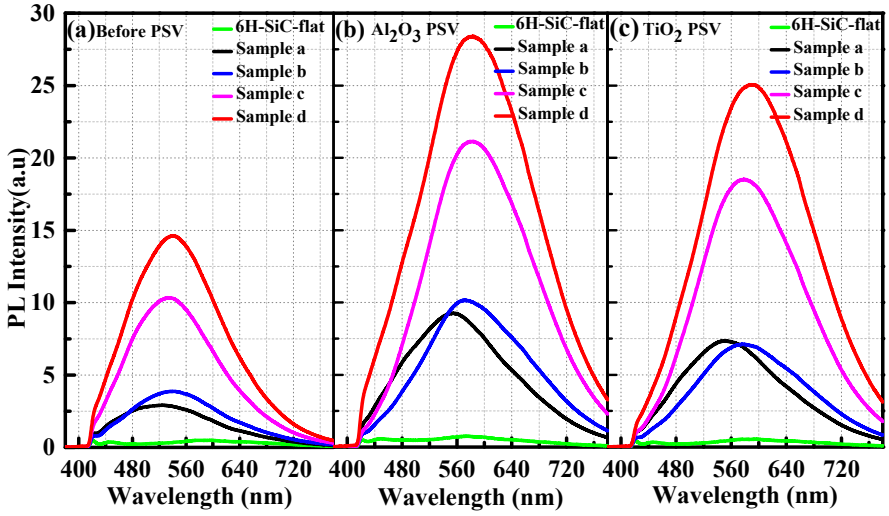

Fig. 6. PL spectra of porous samples (a) with different anodically etching time; (b) passivated by 20 nm thick Al_2O_3; (c) passivated by 20 nm thick TiO_2.

Figure 6(a) shows that the PL intensity increased with the porous layer thickness (anodic etching time) and this trend is directly shown in Fig. 7. The PL spectra with Al_2O_3 and TiO_2 passivation in Fig. (6) show red shifts of approximately 27 nm, 37 nm, 42 nm and 50 nm for samples a, b, c and d, respectively. After Al_2O_3 passivation, the porous samples a, b, c and d exhibit a 222%, 170%, 104% and 94% enhancement, respectively, as shown in Fig. 6(b).

#263004 Received 15 Apr 2016; revised 10 May 2016; accepted 12 May 2016; published 17 May 2016

However, the improvement for TiO_2 passivation is slightly smaller than that for Al_2O_3 films due to the less quantity of O-H bonds [24, 28, 30, 35]. After TiO_2 passivation, the porous samples a, b, c and d have a PL increase of 154%, 83.4%, 78.6% and 71.5%, respectively, as shown in Fig. 6(c). With longer anodically etching time, the thicker of the porous layer formed. And during ALD deposition process, it is difficult for precursors to penetrate uniformly into the deeper layer. Consequently, excess oxygen atoms may exist in the pores and oxidized the porous surface during the annealing process, leading to red shift in porous SiC. Such red shift can be reasonably attributed to the radiative recombination at some oxygen-related defects [36], which were introduced during post-annealing of Al_2O_3 and TiO_2 films.

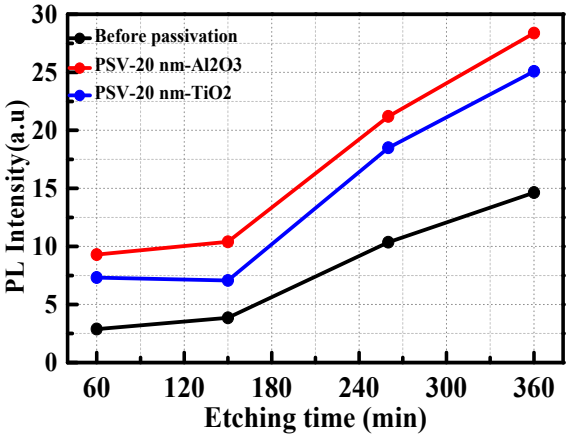

Fig. 7. The relationship between PL intensity and anodic etching time before and after passivation (PSV) by 20 nm Al_2O_3 or TiO_2.

In present experiments, the same thickness was also deposited on both flat Si and 6H-SiC samples. No PL enhancement was observed after thermal annealing, which excludes the emission of TiO_2 films on passivation effect. Moreover, it is worth mentioning that 20 nm for Al_2O_3 and TiO_2 is an optimized thickness, especially for sample d with a 38.8 μm porous layer. Regarding the thickness, the porous layer couldn't be fully filled with thinner Al_2O_3 or TiO_2 films, conversely, the pores maybe oxidized by excess films.

3. Conclusion

In summary, the morphology and optical properties of anodic etched porous SiC has been investigated. Although the origin of the luminescence is not clear at the moment, quantum confinement effects can be excluded and the luminescence is attributed to the surface related effect. We have demonstrated for the first time a significant increase in the PL intensity of porous 6H-SiC passivated by ALD Al_2O_3 and TiO_2 films. These results support the interpretation that surface states are responsible for the light emitting. Compared with the uncoated porous SiC, the Al_2O_3 or TiO_2 coated porous samples exhibit a strong enhancement of photoluminescence, which is attributed to the decrease of non-radiative recombination. Although, the passivation process could give rise to red shift in PL spectra, here we report a effective method to improve the luminescence intensity.

Acknowledgment

This work was supported by Innovation Fund Denmark (project No 4106-00018B).

#263004 Received 15 Apr 2016; revised 10 May 2016; accepted 12 May 2016; published 17 May 2016